Investigation into the effect of the pteroid bone on pterosaur flight

Abstract

The pteroid bone was a wing bone exclusive to pterosaurs. It was fixed to the wrist of all pterosaur species and could be projected forwards during flight or folded inwards whilst the pterosaur was on the ground. A smaller, ventrally projected wing membrane known as the propatagium was fixed to the pteroid and acted as an enlarged leading edge flap. This investigation looked at the effect of the pteroid bone on pterosaur aerodynamics. Experimental conditions were taken from previous wind tunnel experiments and adapted for use in the computational fluid dynamics programs Gambit and Fluent. The results were compared to the previous data and analysed to determine the aerodynamic effects of the pteroid bone. I found that the pteroid bone granted increased lift to the wing especially at higher angles of attack. This meant that the pterosaur could employ the pteroid and propatagium in all flight manoeuvres significantly reducing the effort required to take off, land and maintain flight.

Key words

Pteroid; propatagium; computational fluid dynamics, pterosaur

Aims

- To determine how the pteroid bone was utilised by a pterosaur.
- To investigate the effect of the pteroid bone on pterosaur flight dynamics.
- To compare this data with existing data for conventional wing structures.
- To conclude on its function and effectiveness on pterosaur flight.

Background

Pterosaurs were flying lizards that existed in the cretaceous period and were the first vertebrates to evolve powered flight and they greatly differ from any other flying vertebrate that has existed. They had massive neural network for processing balance information which allowed them to perform complex flight manoeuvres. Evidence for this is found in the enlarged flocculus (New Scientist 1993) which integrates balance information from various parts of the body and sends it to the eyes. The flocculus occupied 7.5% of their total mass, which is significantly more than the 2% found in birds. Current theories suggest that the flocculus had to be enlarged to compensate for their large super-sensitive wings. An increased surface area provided more sensory information, and as such necessitated higher processing power from the brain. Some pterosaurs were covered in a fine hair, making them unique

among reptiles. This suggests that pterosaurs may have been warm blooded, which would give them a much better capability for powered flight.

The pterosaur wing itself was a tough membranous sail like structure that was reinforced by actinofibrillae cords running throughout the cheiropatagium (main wing membrane). These fibres prevent tearing of the wings and acted as a support frame during flight by reducing strain. The cheiropatagium was believed to extend from the end of the forelimb to the rear hind limbs.

Despite their large wingspan and bulky body, the weight of a pterosaur was relatively low. Fossil evidence has shown that *Tropeognathus Robustus* had a wingspan of 6.5 m yet only weighted approximately 13.5 kg. This can be attributed to a fragile, slim bone structure in which many of the bones were fused together. Most notably the notarium, where the fused backbone stiffened the torso during flight and provided a stable support for the shoulder blade. Their bones were hollow thus reducing their bone mass considerably meaning that they broke easily. There are very few specimens with complete wing structures, and even fewer with complete skull. Over time, sediments piling up on the bones would cause them to collapse and fragment.

The pteroid bone was a structure attached to the pterosaur wrist and has been viewed as an evolutionary step in the advancement of pterosaur flight. The actual origin of the pteroid is not certain. It has been suggested that the structure could be a modified carpal, the first metacarpal or a genetic anomaly known as a neomorph (Unwin 1996).

Williston (1891) was the first to suggest that the pteroid bone was not a digit. He argued that the phalangeal layout of the carpals did not corresponding to any other reptiles when the pteroid was included. His paper started a protracted debate that continues to this day.

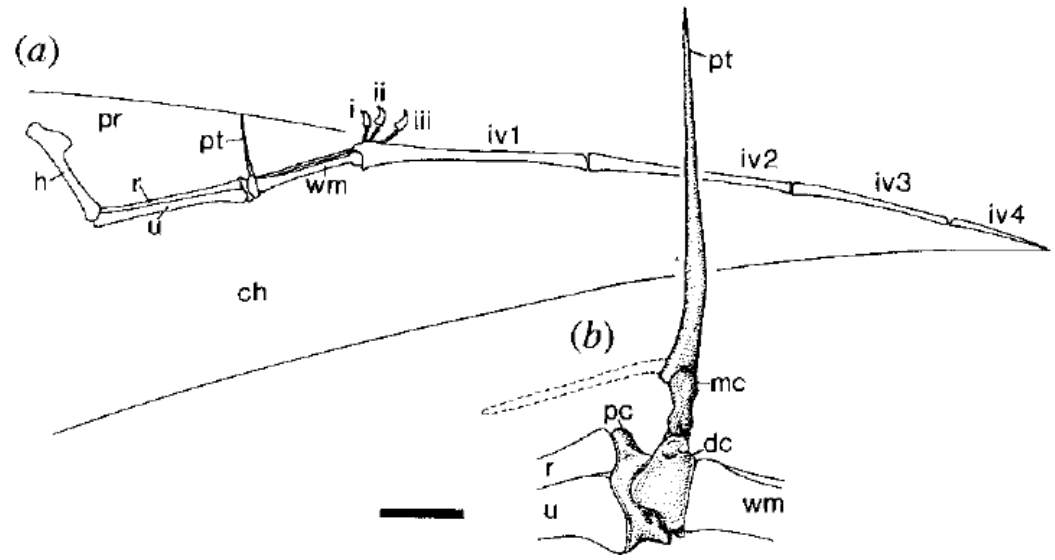

Fig. 1 – (a) Forelimb of *Tropeognathus Robustus* (SMNK 1133PAL) (Unwin 1996) with ventral pteroid arrangement
(b) Pteroid schematic

Studies have shown that the structure is however a true bone that served some function in the mechanics of flight. Modern counterparts of the pteroid bone could include the alula found in birds or slats found in fixed wing aircraft. The alula is homologous to the thumb and is used to delay stall during takeoff and landing in birds.

Fig. 1 shows the arrangement of the forelimb of *Tropeognathus Robustus* (SMNK 1133PAL). The complex articulation of the pteroid with the medial carpal and distal syncarpal shows that the pteroid bone did indeed have some degree of movement. The discovery of pronounced muscle attachment sites are further evidence that the bone could be orientated at will. This also suggests that a forward projected wing membrane, called the propatagium was attached to the bone. Further evidence for this is found through a leading edge muscle similar to that of a bat's occipitopollicalis muscle. However this muscle would attach from the leading edge to the base of the skull, which is not feasible for any of the pterosaurs, because their necks were too long. According to Bramwell and Whitfield (1974), the pteroid muscle originated on the fore part of the sternum and was controlled alongside muscles in the neck. Their paper assumes that the pteroid was directed toward the body and does not address the question of the bone's function. Based on anatomical models though it is obvious that the pteroid was indeed strong enough to withstand the rigours of flight since most of the strain exerted upon it would be absorbed by the muscles surrounding it.

There has been great difficulty in determining the absolute function of the pteroid bone due to the number of different anatomical arrangements of each specimen. Species such as the *Pterodactylus kocho* (BMNH 42736) which possessed some of the latest evolutionary changes, had an under-developed pteroid bone. Studies by Unwin (1996) have shown that many species did not utilise the pteroid bone until full maturity, when their bones were completely ossified.

Until the early 1980's, it was widely believed that the pteroid pointed medially (towards the body) (Bramwell and Whitfield 1974; Wellnhofer 1985, 1991a) because the majority of articulated, flattened fossil skeletons showed this as true. However, having the pteroid projected medially would not provide any significant benefits to pterosaur flight since its range of movement would be limited by the attached propatagium. Frey & Reiss (1981) argued that the pteroid bone was directed antero-ventrally (forwards and downwards) during flight, and could be manoeuvred vertically according to the required flight dynamics thus creating a new wing profile shown in Fig. 3. Here we can see that the propatagium extends forwards quite significantly and since it is connected to the pteroid, the propatagium could be directed up or down during flight to form a different wing profile.

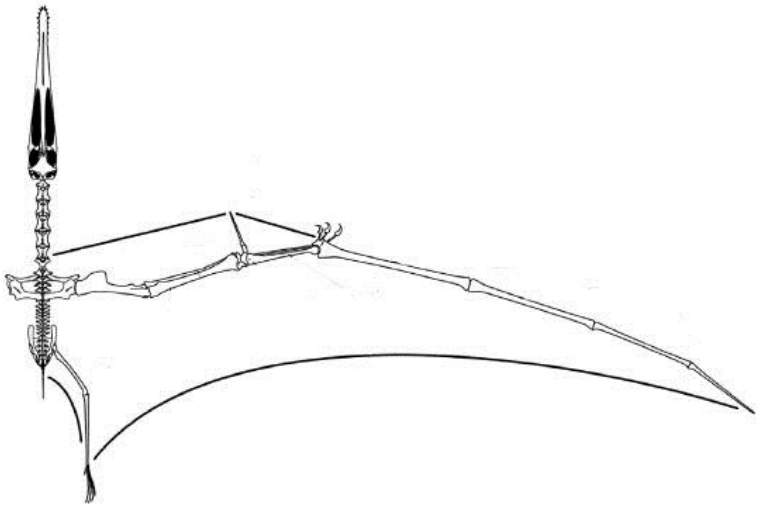

Fig. 2 – *A. Santanae* (AMNH 22555) adapted from Wilkinson (2005)

Studies have shown that unlike current flying animals, pterosaurs had lost the capability of voluntary motion of their interphalangeal joints (Bennet S.C. 2001). This severely limited the movement of the wing finger (fourth metacarpal), and as a result would have limited the movement to a simple flap. Certain flight manoeuvres, such as rolling, would have been extremely difficult if not impossible. However, this increase in rigidity of the pterosaur wing would decrease the likelihood of damage during high speed flight and landing.

The flight mechanics of pterosaurs was completely different to all other flying vertebrates. Birds for example control their flight through their tail feathers, using them as a rudder for balance and steering. Whilst soaring, the tail feathers are extended to provide a greater surface area and increase lift and also the tail could be directed downwards, acting as an airbrake whilst slowing down. In contrast, pterosaurs did not have a tail wing at all. This raises a number of questions as to how they could control various aspects of flight, primarily slowing down and steering. To compensate for this apparent lack of yaw control provided by a tail, skeletal reconstructions of *A. Santanae* have shown that it possessed an elongated crest on its head much like a small fin. This would have allowed the pterosaur to improve its steering capability but not enough to provide total control of yaw (Wellnhoffer 1991b).

There are two hypotheses concerning terrestrial motion of pterosaurs. Early reconstructions of the first specimens incorrectly included a wing membrane situated between the hind legs (Soemmerring 1817). This model was erroneously based upon that of a bat and it was believed that the fossils belonged to an aquatic rather than airborne dinosaur.
Unfortunately, Soemmerring's incorrect reconstruction influenced a century and a half of palaeontology and its influence can even be seen in some relatively recent studies (Padian 1981). The presence of this extra membrane would significantly complicate walking for the pterosaur tying the legs together.

The analysis of numerous fossilised skeletons has shown that no pterosaurs actually possessed a wing between their hind legs. Functional analysis of the skeleton of *A. Santanae* (Wellnhoffer 1991b) shows that pterosaurs were quadrupedal, with their forewing folding back on itself and the

metacarpals in contact with the ground. To facilitate this, the pteroid muscle can be pulled taught thus drawing the forewing inwards and lowering the walking profile of the dinosaur. It is believed that the pterosaur would remain on all fours whilst stationary to reduce the stress put on their hollow bones. However, they would have had trouble running at high speed whilst quadrupedal.

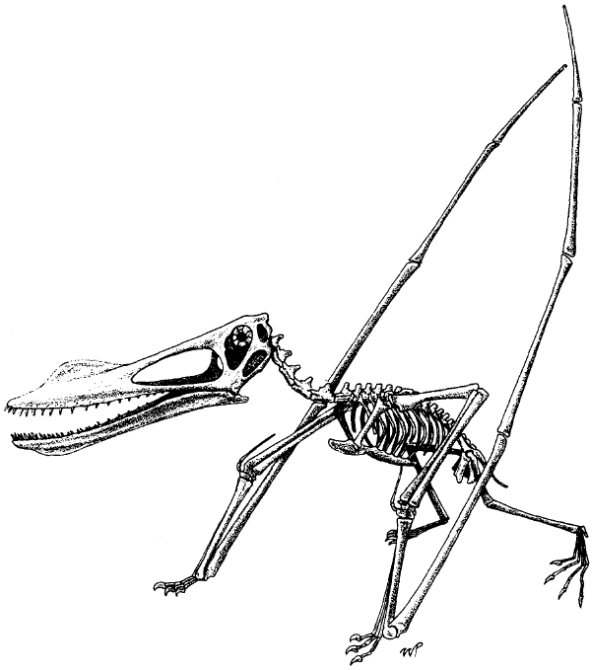

Fig. 3 – *A. Santanae* reconstruction (Wellnhoffer 1991b)

The pteroid bone is clearly visible oriented parallel with the wing metacarpal in Fig. 3. Also the crest to the front of the nasal cavity is visible. The crest visible here is significantly smaller than other pterosaur species, most notably *Pteranodon Ingens* (Stein 1975) which had a crest as large as the head itself. The hind limbs are clearly in a digitigrade position with only tip toes in contact with the ground.

Current theories suggest that *A. Santanae* would switch from plantigrade (feet flat) to digitigrade (tip of toes) motion depending on the circumstances. The forewing could be “snapped” into flight position, and the pterosaur would rear up plantigrade. Takeoff would be similar to that of fixed wing aircraft with the pterosaur having to reach takeoff velocity (Stein 1975) before it could get airborne. However, a running take off would alter the angle of attack of the wing with every step. To overcome this, the pterosaur would have to raise and lower its wings simultaneously; however it is doubtful the weak leg bones could support such a rigorous action as running (Williston 1891) and as such this theory seems unlikely.

Bramwell (1970) proposed that pterosaurs would simply raise its wings while facing a head wind. Again there are problems with this theory; the boundary layer of the ground reaches above the height of the pterosaur thus producing turbulence and decreasing velocity. Therefore the only viable conclusion was for a gravity assisted take off similar to those used in hang gliding. The pterosaur would have to stand on the edge of a cliff or on top of a

hill and “leap” into the air. This theory, whilst dealing with all the shortcomings of take off, would have doomed the pterosaur to a “Flying Dutchman” existence (Greenhalgh *et al* 1984). Landings for pterosaurs would almost certainly mean death unless they could find a suitable ledge to jump from again since without flight, the pterosaur would be very vulnerable to predators.

Evidence for the wing snapping into position is shown in Fig. 4 by Bramwell and Whitfield (1970). The notch in the shoulder would “click” in place when the pectoral muscles were flexed. This would give a significant increase in wing stability during gliding.

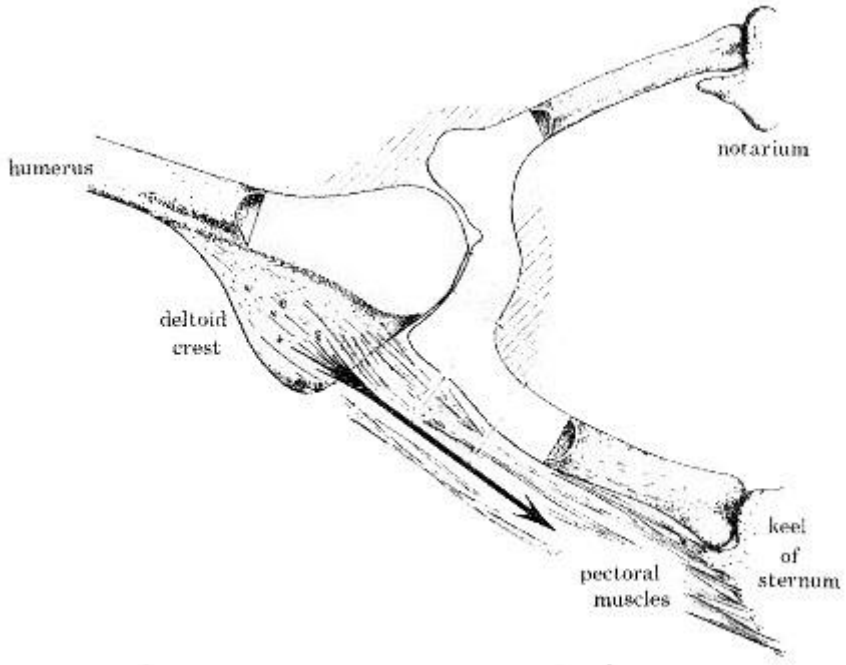

Fig. 4 – The wing (humerus) joint with the shoulder adapted from Bramwell and Whitfield (1974)

This investigation will determine the flight benefits provided by the pteroid bone. The wing profile used is based upon *A. Santanae* (AMNH 22555) reconstructed by Wellnhoffer (1991b) and adapted by Wilkinson (2005). Analysis of different wing profiles will show how the inclusion of a propatagium would aid flight, and the added manoeuvrability it gave.

A similar study undertaken by Wilkinson (2005) was able to model forces on the wing using wind tunnel testing. In his paper, “High lift function of the pterosaur forewing”, Wilkinson was first to incorporate a forward facing pteroid bone into flight dynamics calculations. The apparatus included an aluminium tube as the wing spar and a nylon sheet as the membrane. In his reconstruction of the wing, Wilkinson has assumed that the propatagium extended from the pteroid to the first metacarpal, providing a continuous leading edge from the sternum to the metacarpals. Whilst there has been little evidence to suggest this, it is unlikely that a prominent gap would exist between the bones because this would lead to aerodynamic complications during flight. Numerous investigations into general pterosaur flight have been undertaken and will provide further experimental data comparisons. The most comprehensive flight analysis is that of *Pteranodon Ingens* (Stein 1975).

Methodology

Data for the wing profiles was sourced from Wilkinson (2005) and experimental conditions from Stein (1975). Testing was conducted using the modelling software Gambit and the solver Fluent. By varying the angle that the propatagium makes with the cheiropatagium, the effect of the pteroid bone on flight dynamics could be determined. The dimensions of the wing profile to be implemented were taken from Wilkinson (2005).

Table 1 – Key dimensions taken from Wilkinson (2005) model

model	chord (m)	span (m)	spar diameter (m)	spar leading edge (m)	spar trailing edge (m)
no forewing	0.173	0.706	0.016	0	0.166
broad forewing	0.218 – 0.239	0.706	0.016	0.073	0.166

The wingspan that had been constructed was 706 mm in length. The model has a wingspan of 4 m in this investigation and so the values required were scaled up accordingly. A figure of 4 m is comparable to that of specimen AMNH 22555 (Wellnhoffer 1991b), which had a wingspan of about 4.5 m and served as a model for previous studies (Wilkinson, 2005).
The following table shows relative dimensions to begin construction of the wing profiles.

Table 2 – Key dimensions required for profile construction

model	chord (m)	span (m)	spar diameter (m)	spar leading edge (m)	spar trailing edge (m)
no forewing	0.980	4.000	0.091	0.000	0.941
broad forewing	1.354 (max)	4.000	0.091	0.414	0.941

The values in Table 1 and 2 correspond to the dimensions shown in Fig. 5.

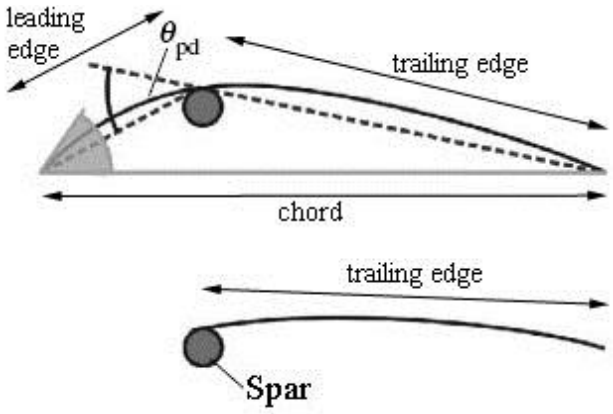

Fig. 5 – Simplified wing profile according to Wilkinson (2005)

The lower diagram in Fig. 5 shows the wing model without a propatagium. The results obtained from analysing the upper diagram can be compared to this in order to determine how the pteroid affected

aerodynamics. Altering the angle θ_{pd}, is equivalent to positioning the pteroid further downwards.

The mass of a pterosaur can only be estimated from fossil records. The square cube law relating wing span to loaded mass is a useful tool for estimating loadings for a given flight type. The three categories of flight dynamics are conventional flying devices (modern airplanes), soaring birds and sailplanes, and finally low wing loading ultra light types e.g. hang gliders (Greenewalt 1962). All species of pterosaur would fall in the low wing loading category since the size of their wing is large compared to that of their body. Greenewalt's equation is:

$$M = (1.2 \pm 0.6).S^{\frac{3}{2}} \quad (1)$$

Where M = loaded mass and S = wing area. This equation gives the theoretical maximum load that a wing area could lift. Taking the assumption that the wingspan will be 4 m and data from Table 2, the relevant loadings for each model were determined (Table 3).

Table 3 – Approximate wing loadings

	Area (m^2)	Min. load (kg)	Max. load (kg)
No prop.	3.776	4.4	13.21
Propatagium	5.416	13.61	22.69

The pterosaur weight was calculated from the average of the figures for each model, 8.81 kg for the simple model and 18.15 kg for the propatagium model. The results raise some questions about the suitability of this equation for the different wing profiles. The equation can only be related to congruent wing profiles, meaning that one of the results is incorrect. By adding the propatagium, the mass of the pterosaur would only slightly increase yet the theoretical loading could almost double. Since the ranges of loadings do not overlap, previous investigations concerning pterosaurs must be studied. Other studies have shown that *Tropeognathus Robustus* had a wingspan of 6.5 m (Wellnhoffer 1991b). Reconstruction of the fossilised remains has shown that the approximate weight of the specimen was 13.61 kg (30 lbs). Scaling this value for a 4 m wingspan, a weight of 8.38 kg was obtained. However, this species of pterosaur is different from *A. Santanae* since they differ slightly in their anatomy (Wellnhoffer 1991b).

When data from Wellnhoffer (1991b) was compared to Greenewalt's approximation, there was less than a 5% difference to the average mass loading value for the basic model.

Therefore the calculated mass of the pterosaur was assumed to be 8.81 kg. The mass of the pterosaur was not required in the calculations because it does not affect the profile of the wings. It did however serve as a comparison to the potential lift generated by the wings. A detailed list of specimens' weights and wingspans can be found in appendix (a).

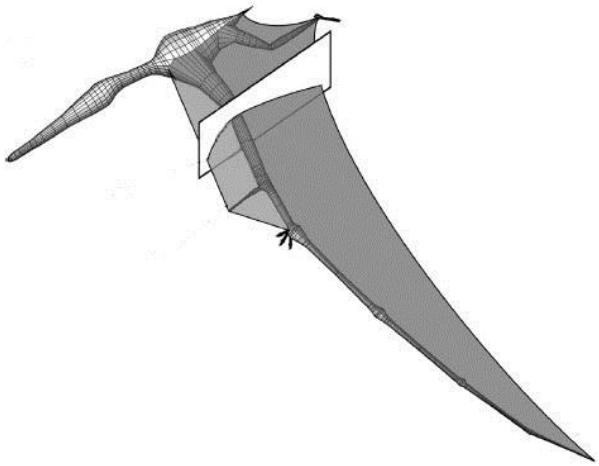

Fig. 6 – *A. Santanae* 3D computer model adapted from Wilkinson (2005)

Fig. 6 is a 3D model of the *A.Santanae* pterosaur. The cross section is taken from the midpoint of the propatagium, perpendicular to the wing spar.
The height of the wing was quantified with the excess length ratio parameter.

$$\varepsilon = \frac{l - c}{l} \tag{2}$$

Where: L = wingspan, c = chord.
The models created have an excess length ratio of 0.04, which is comparable to that used in Wilkinson (2005) and is a common value used in many airfoil designs (Newman and Low 1984).
There are seven different models to be analysed: a profile without a propatagium, and six models with a propatagium with θ_{pd} from 10° to 60° in 10° increments. The wings were fixed, with no allowance for slackening to negate the extension of the membranes and obtain absolute results. However this required the profiles deviate away from a curved shape.

Fig. 7 – Gambit image of 30° wing profile

Fig. 7 shows the 30° propatagium model as constructed in Gambit. Taking data from Table 2, it was possible to determine the coordinates of the wing vertices using trigonometry appendix (e).

Once the coordinates of the wing were inputted into Gambit, the conditions of the outer boundary could be determined. In the previous study using wind tunnel testing, the physical boundary imposed on the apparatus was a closed test section 0.71 m wide by 0.51 m high. When compared to the data, the boundary used is approximately four chord lengths wide by three chord lengths high. Whereas for this investigation the test area was two chord lengths high by five chord lengths wide, thus allowing a greater area of analysis. An increase in the boundary width is required to distance the interaction of the flow with the wing profile from the inlet, thus preventing non-

uniform stagnation effects as the flow is “backed up” at the air inlet. The inlet was set as a velocity inlet and the exit boundary of the domain set as a pressure outlet. This results in a better rate of convergence should backflow occur during the iteration. The upper and lower limits of the boundary were set as periodic conditions allowing the boundary area to be replicated throughout space to form an infinite lattice. This means that the system effectively has no surface or ends so ground effects can be neglected. To create the walls of the wing profile, the outer boundary face was retained, and the airfoil subtracted from it. The final step was to mesh the face. For this, approximately 8000 cells were required, with increasing mesh complexity close to the wing wall.
The required number of nodes for this many cells is shown in Table 4.

Table 4 – Approximate required edge mesh for 8000 cells.

Boundary	Edge mesh value
Wall	10
Velocity inlet	20
Pressure outlet	20
Periodic	40

Owing to the triangular dimensions of the wing profile, the mesh utilises triangular cells. Triangular cells allow for a gradual increase in mesh density from the boundary edges to the wing wall by allowing cells to be clustered in selected areas of the flow domain (i.e. close to the airfoil). The triangular cells also significantly improved the skewness observed for the mesh; the dimensions of the cells were similar to their adjacent for the triangular mesh.

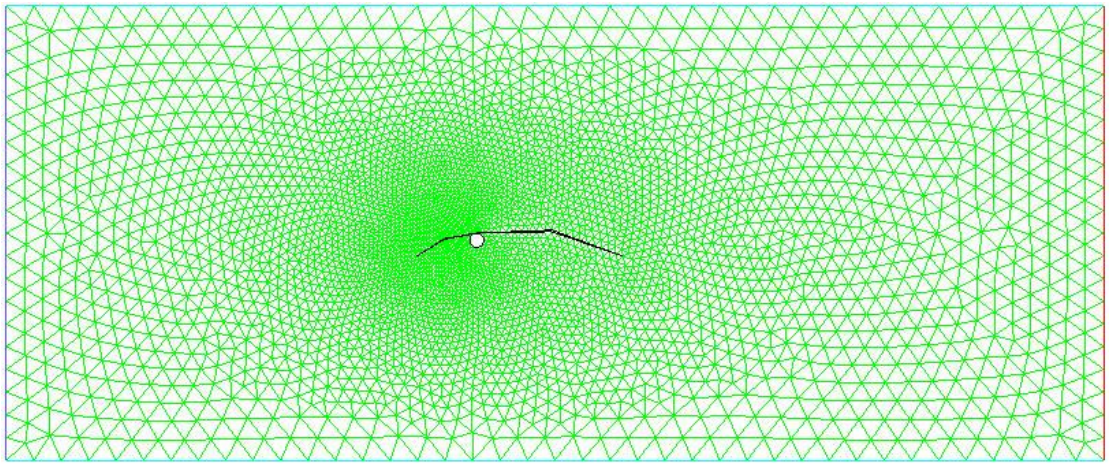

Fig. 8 – Mesh of 30° propatagium model with approximately 8000 cells taken from Gambit

The completed mesh was exported to Fluent, which allowed the modelling of fluid flow. Fig. 8 is a completed mesh with a greater density nearer to the wing wall where greater accuracy is required. A number of conditions and requirements needed to be specified in order to obtain accurate results. The most obvious was the flow velocity and the fluid itself. Wilkinson (2005) utilises a Reynold’s number of 1.2×10^5. This can be inputted into Fluent using the Reynold’s equation;

$$\mathrm{Re} = \frac{VL}{\nu} \tag{3}$$

$$V = \frac{15.11 \times 10^{-6} \times 0.091}{1.2 \times 10^{5}}$$

$$V = 19.93 ms^{-1}$$

The onset of turbulent flow occurs at a Reynold's number of 2300. At an air speed of 19.93 m/s, the flow is clearly turbulent.
The air was assumed to be at 20°C with a density of 1.225 kg/m^3 and kinematic viscosity 15.11 x 10^{-6} m^2/s, in accordance with experimental procedures from Wilkinson (2005) and sourced from steam tables (Rogers and Mayhew 2003). Since the flow is turbulent, the viscous solver was set to a standard k-epsilon model. This is used rather than the RNG or realisable model due to its higher level of consistency. Problems with the standard model could potentially include adverse pressure gradients or stagnation point anomalies but the relative simplicity of the model negates these issues. The standard model is somewhat more valid than the other models due to its simpler numerics for a simple 2D case such as this.

The solution controls were initially set to first order upwind discretisation and can be used to improve convergence by shifting to second order upwind should the model fail to converge. First order quantities assume that the cell-centre values of a variable signify an average value for that cell. As a result, the value is constant throughout the entire cell.
Accurate convergence values are paramount in obtaining correct results. Therefore convergence values were decreased two orders of magnitude to 0.00001 for each of the criteria.
Rather than alter the angle of the wing the angle of attack can be changed by varying the x and y components of the inlet airflow. Altering the wing's angle would have required hundreds of meshes to be constructed, all with varied cell meshes. By using simple trigonometry, the airflow could be directed at any angle specified, thereby removing the need for multiple meshes for each case. Wilkinson's investigation studied angles of attack between -2° and 20°. To obtain comparable results, angles from 0° to 20° in 2° increments were recorded. A table of the required angles of attack with the corresponding velocity components is shown in appendix (b).

The solution was initialised from the velocity inlet since the velocity is the only variable for each model. The number of iterations was set to 5000, since this would be more than enough to achieve convergence for the models.

The primary experimental data retrieved from the model analysis was the lift and drag experienced by the wing profile. Lift is defined as the total force experienced by the wing perpendicular to the flow of air. Similarly, the drag encountered by the wing is defined as the total force incident upon the wing parallel with the flow of air. Since this is a 2D case, the only drag experienced by the wing will be profile drag. Induced drag is not applicable for this model since the wing is theoretically of infinite length and so is not accounted for in the experimental procedure.

Fluent can report the forces experienced by the wing in any given direction. Table 8 in the appendix (c) shows the force vector inputs required for each angle of attack the wing undergoes. The results obtained from Fluent

can be implemented into the lift and drag equations. Fig. 9 is a schematic diagram of the lift and drag forces experienced by an airfoil when subjected to a flow of air. Note the lift and drag are always perpendicular to each other.

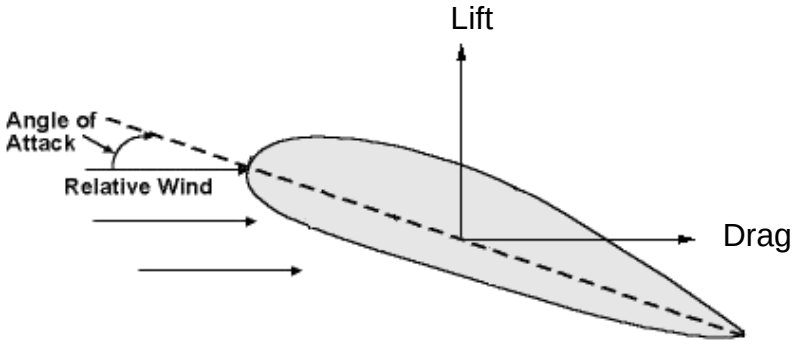

Fig. 9 – Schematic diagram of forces on an airfoil in an airflow.

The results obtained from Fluent can be implemented into the lift and drag equations.

$$C_L = \frac{2L}{\rho \cdot V^2 \cdot A} \tag{4}$$

$$C_D = \frac{2D}{\rho \cdot V^2 \cdot A} \tag{5}$$

Where: L = lift force, D = drag force, C_L = coefficient of lift, C_D = coefficient of drag, V = air velocity and A = wing area.
The wing area for each model is equivalent to the chord length for both propatagium and cheiropatagium multiplied by the wingspan. This equates to an overall wing area of 5.416 m^2 for the pteroid model and 3.776 for the basic model.

To investigate the accuracy of the results, comparisons were drawn between previous studies by Wilkinson (2005) and Stein (1975). However there is no guarantee that the conditions used will provide the most accurate results. To determine how the operating conditions specified above affected the forces experienced by the wings, a number of changes were implemented. The 30° propatagium model was selected for further investigation since its dimensions are approximately average when compared to the other models. Primarily, the cell mesh was increased from 8000 to 18000 cells. This was achieved by doubling the edge meshes on the wall and boundary. Increasing the mesh density increases the computing power required to analyse the flow and increases the accuracy of the simulation by improving the grid's smoothness. Smoother grids allow for a reduction in any truncation errors by reducing the change in cell area, thus producing more accurate results. Fig. 10 shows the 30° propatagium model with a refined mesh. Note how the change in cell area is decreased when compared to the standard mesh in Fig 8.

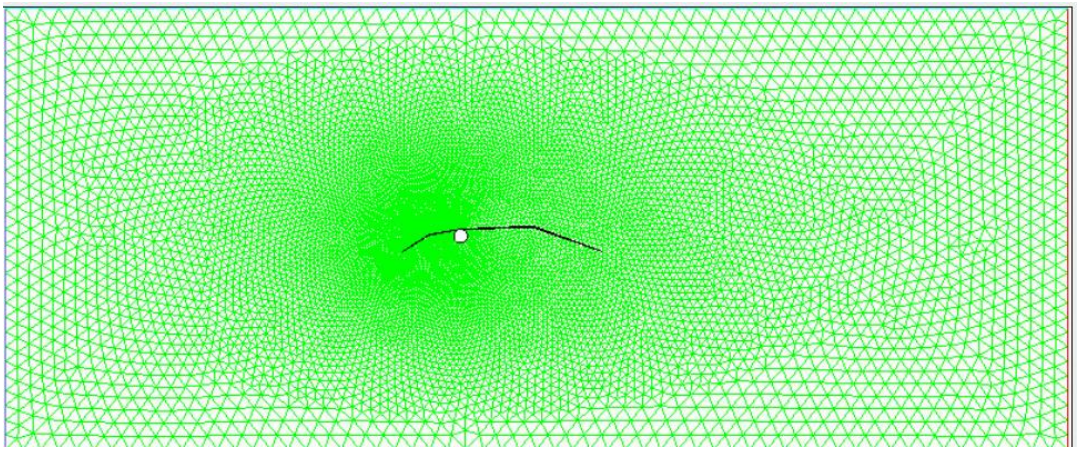

Fig. 10 – Mesh of 30° propatagium model with approximately 18000 cells taken from Gambit

Further refinements to this model were made by altering the discretisation factors. By changing from first to second order upwind discretisation, the values at the cell faces are computed using a multidimensional linear reconstruction. This is effectively done by using a Taylor series expansion of the cell centre solution and applying it to the cell faces. Combining the mesh refinement with this second order discretisation would theoretically increase the accuracy of the results. As stated earlier in this report, the turbulence model used was standard k-epsilon. The 30° propatagium model was also solved using an inviscid and a k-omega viscous model as a comparison.

The wing spar to which the cheiropatagium and propatagium are attached is a significant aerodynamic boundary. The models were also solved with the spar not included to determine any differences in aerodynamic performance.

Results

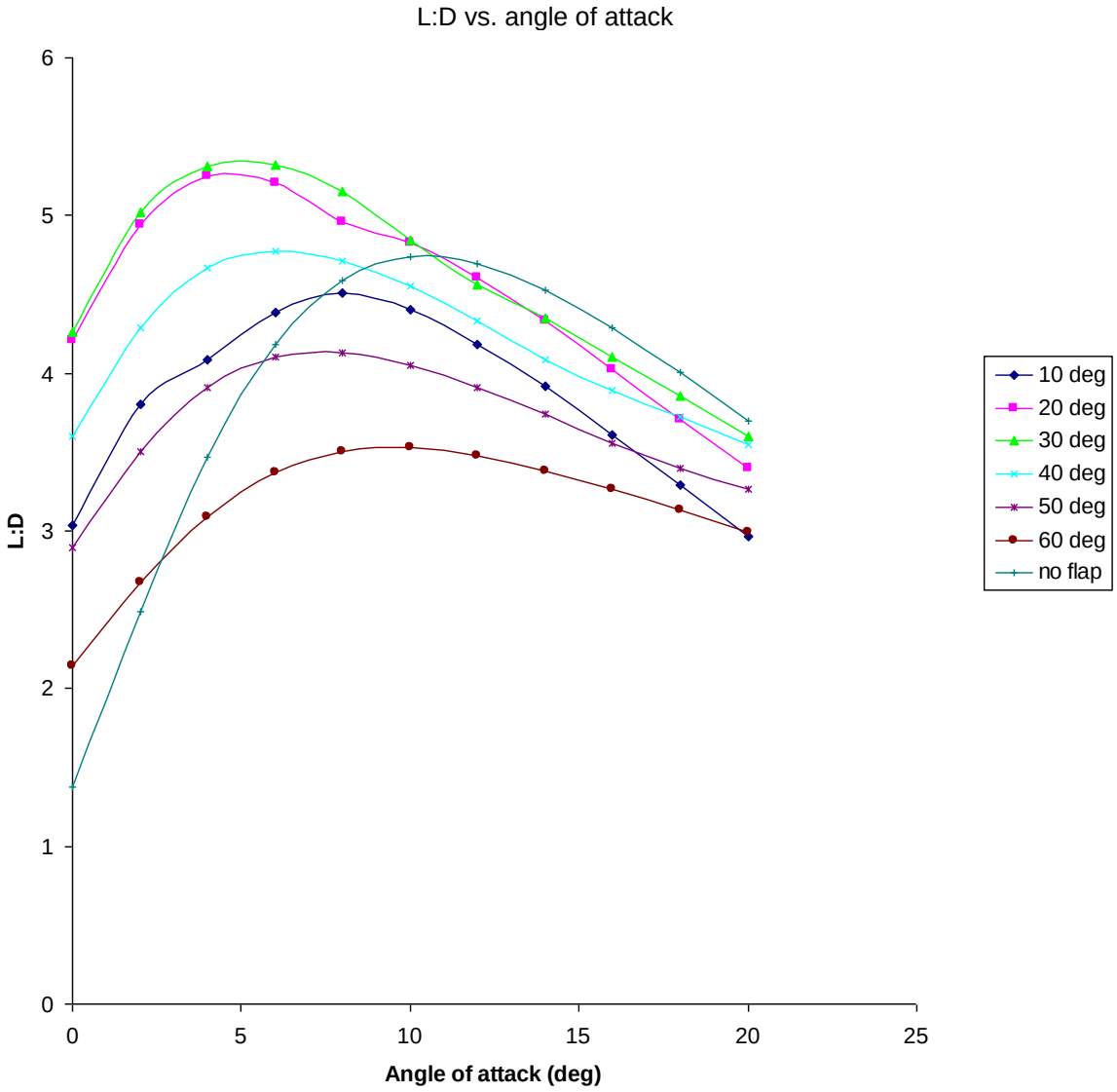

Fig. 11 – Graph showing L:D ratio as a function of angle of attack for varied θ_{pd} and basic model

The 30° model performed excellently due to its compromise between an increased camber and slim profile. The large profile of the 60° model performed poorly at high angles of attack. The air flow was almost perpendicular at incidence, thus increasing the pressure at the wing wall as its velocity decreased, thus increasing drag.

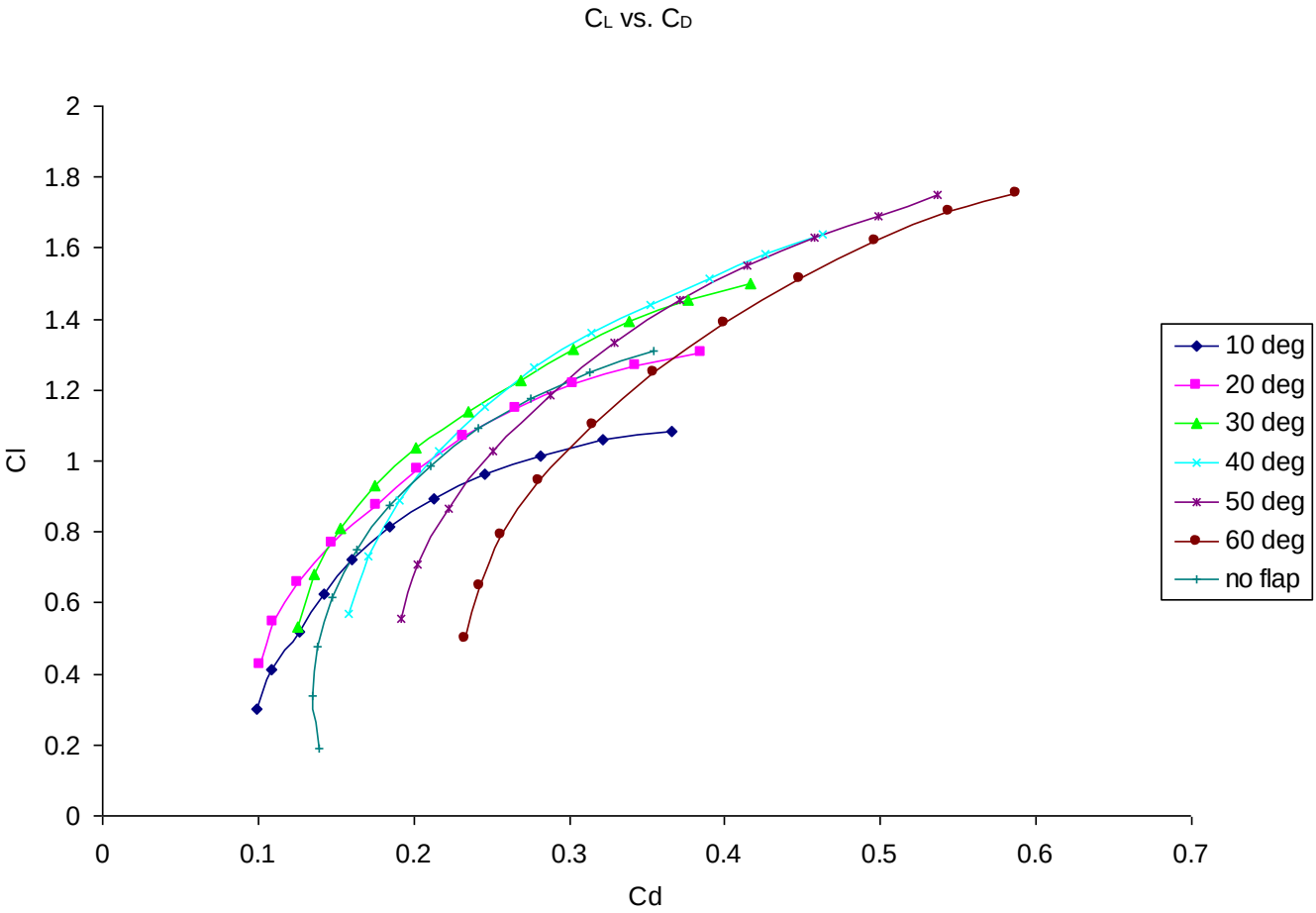

Fig. 12 – Lift coefficients as a function of drag coefficients for all θ_{pd} angles and for basic model

At higher angles of attack, the lift coefficients were markedly better for propatagium models (Fig. 12) with a θ_{pd} of 30° and above. Peak values for C_L are approximately 1.75 for the 50° and 60° models, a significant improvement over the 1.3 achieved by the simple model. Very high C_D values are shown for each model. However the lift coefficient values are considerably lower than those achieved in the Wilkinson (2005) study, where peak values of 2.4 were obtained. Table 5 shows the peak L:D values obtained for each model. This ratio is a measure of how efficiently the wing produces lift. The values shown are extremely poor compared to those obtained by Wilkinson (2005), where the peak value was 18. When compared to Stein's (1975) investigation, the values in table 5 are similar to the mid range expanded wing test models. All values shown neglect the drag created by the animal's body, which would increase the C_D, decreasing L:D further.

Table 5 – Peak L:D values for each modelled wing profile

	Peak L:D
no prop	4.74
10 deg	4.5
20 deg	5.25
30 deg	5.32
40 deg	4.77
50 deg	4.13
60 deg	3.53

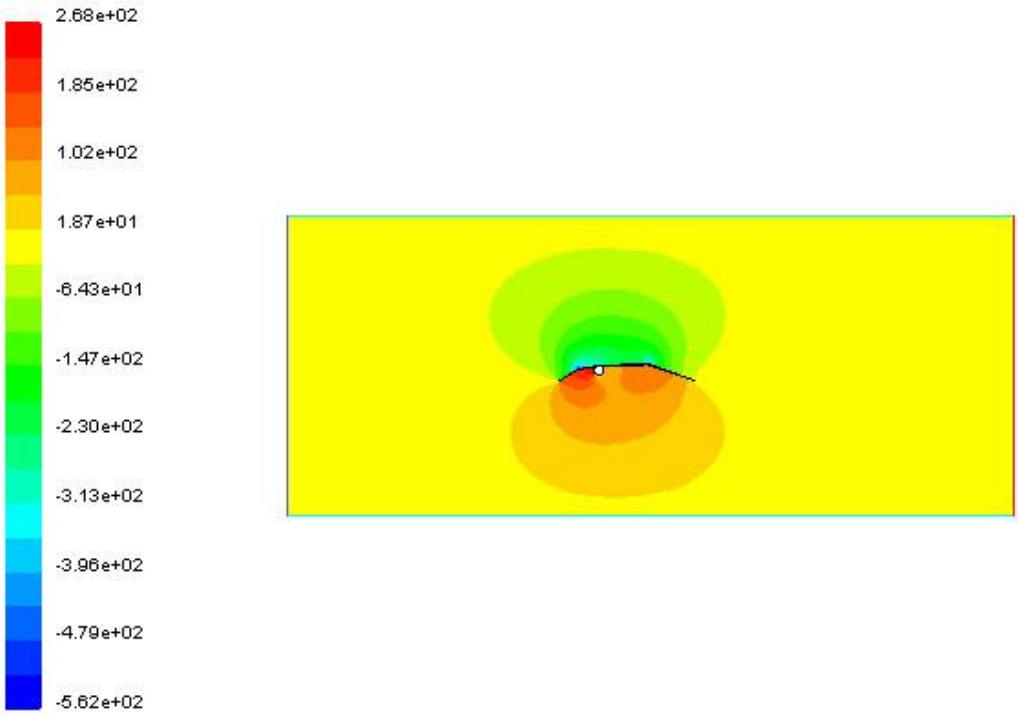

Fig. 13 - Contours of static pressure (Pa) for 30° propatagium model at 16° angle of attack taken from Fluent.

Fig. 13 shows contours of static pressure for the 30° model. This model clearly shows the distribution of pressure forces beneath the wing profile. The highest pressure is situated at the joint of the pteroid, where the propatagium meets the wing spar.

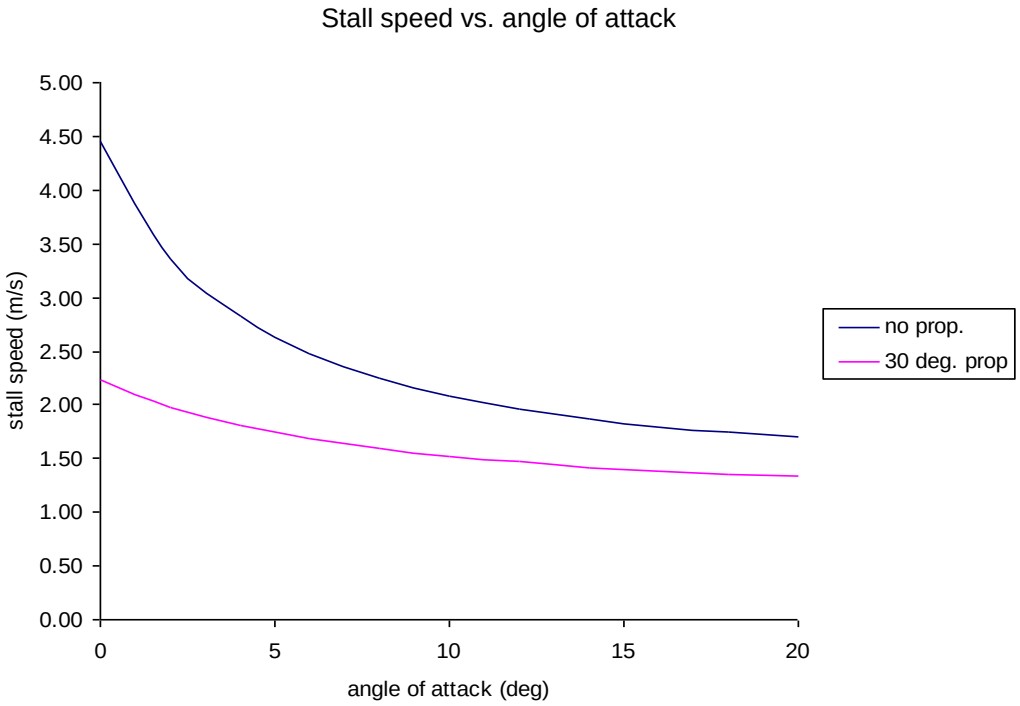

Fig. 14 – Comparison of stall speeds for varied angles of attack for 30° θ_{pd} and basic model

Fig. 14 shows how the stall speed is reduced with a propatagium. This allows the pterosaur to maintain flight at slower speeds, and also reduces the air velocity required for takeoff. The improvement is greatest at lower angles of attack and can be attributed to the increase in wing area. It is worth noting that for other angles of the propatagium, the increase in camber has relatively little effect on the stall speed of the wing since the difference between C_L is lower than that of the wing area for all propatagium models.

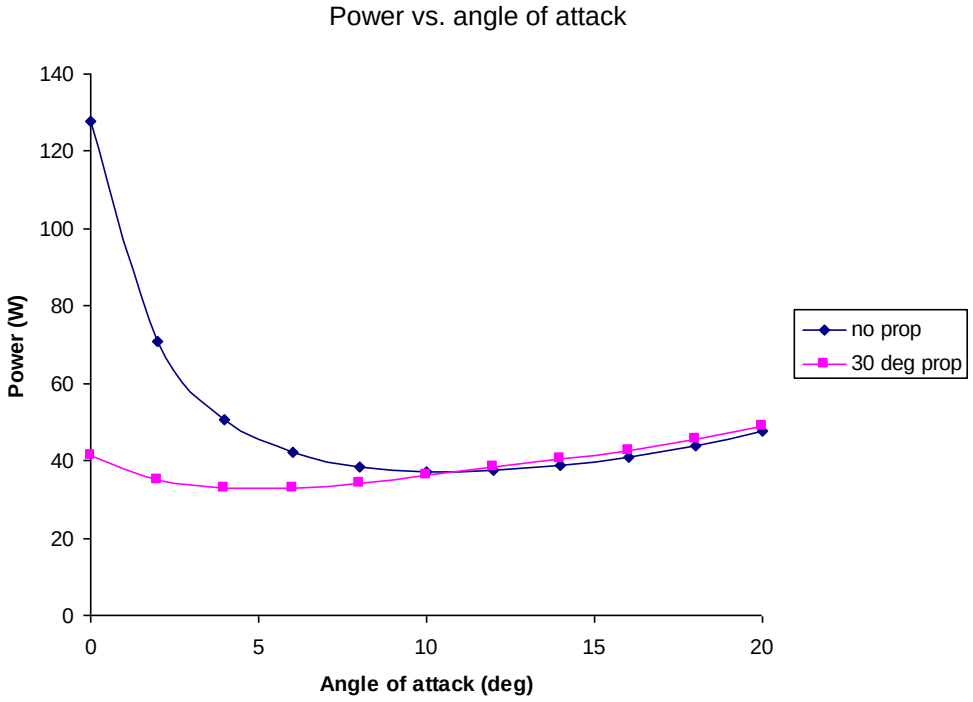

Fig. 15 – Power requirements for pterosaur flight for 30° θ_{pd} and basic model

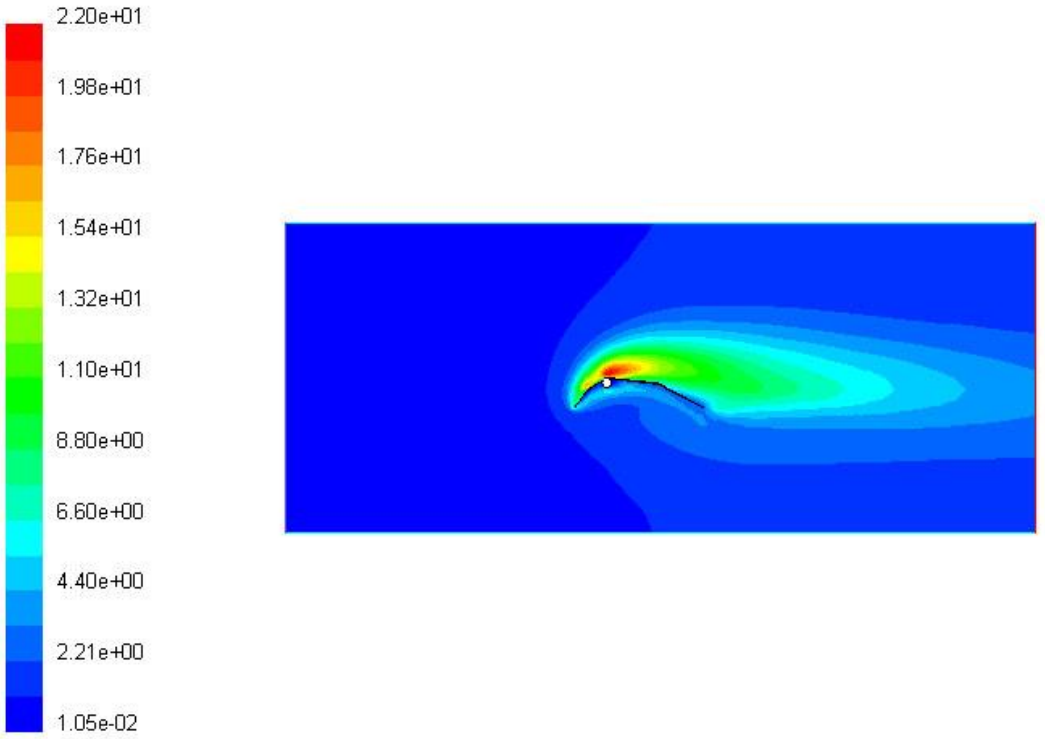

Fig. 16 - Contours of turbulent kinetic energy (m^2/s^2) for 60° propatagium model at 16° angle of attack

The red area represents high turbulent kinetic energy, suggesting that a reverse vortex has been shed, cancelling the bound vorticity at the trailing edge of the wing.

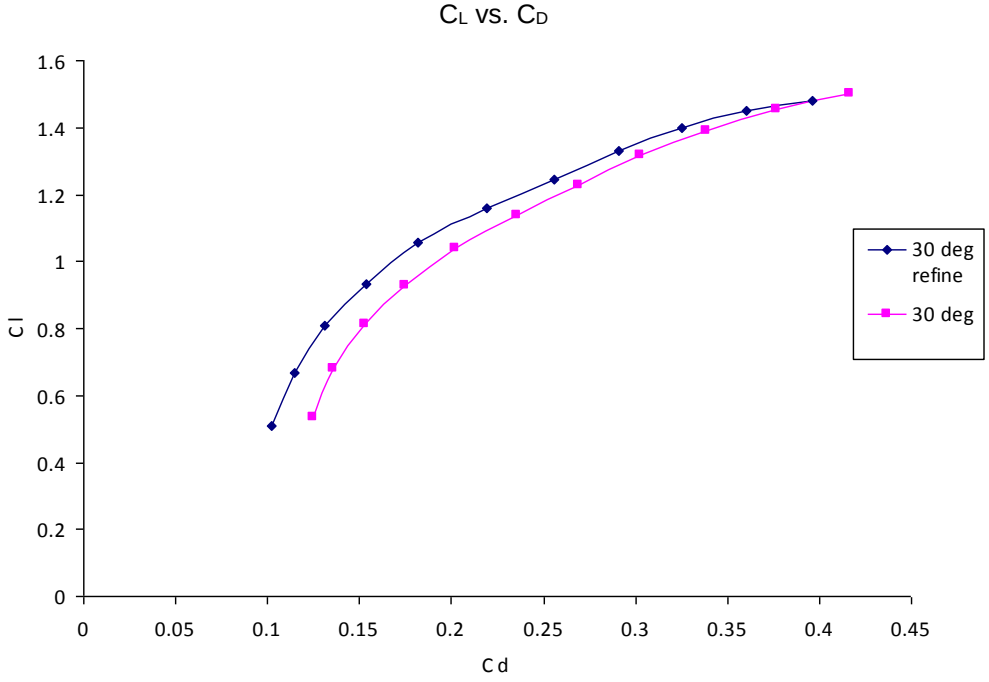

Fig. 17 – Comparison of 30° simulations for 30° θ_{pd} and basic model

Fig. 17 shows the effect of refining the mesh and changing the discretisation factors to second order upwind for the 30° propatagium model.

The recorded lift coefficients only show minimal reductions whereas the drag coefficient is reduced by approximately 5%.

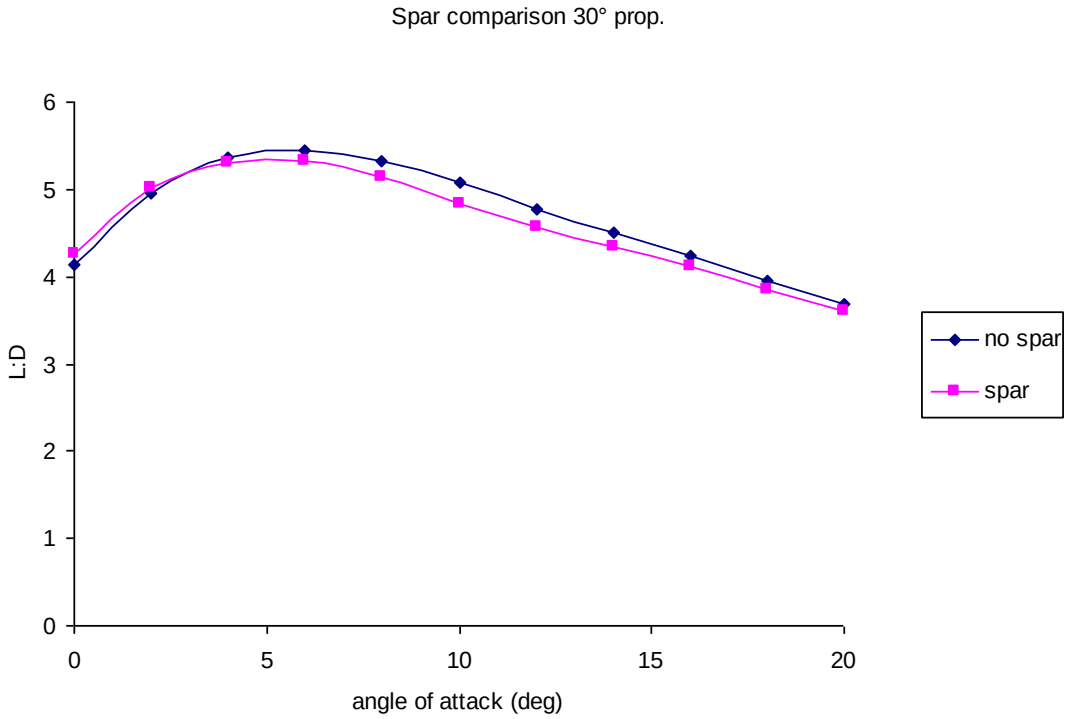

Fig. 18 – Flight efficiency comparison for 30° propatagium model for 30° θ_{pd} and basic model

The removal of the wing spar has very little effect on flight efficiency for the propatagium model. Removing he wing spar for the basic model significantly increases the available lift, especially at lower angles of attack. A peak L:D value of 9.3 is available as shown in Fig. 19.

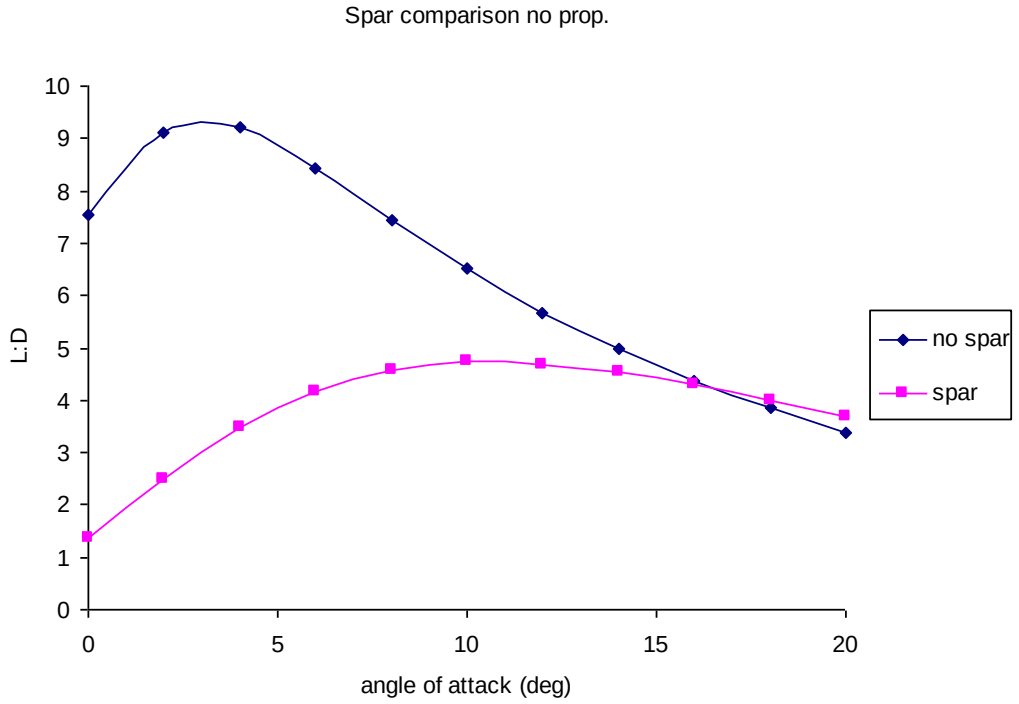

Fig. 19 – Flight efficiency comparison for basic model without propatagium

Analysis

The results show that the inclusion of the pteroid bone in flight afforded the pterosaur increased lift, especially at higher angles of attack. The L:D ratio is superior for all propatagium models for angles of attack below 12°, as shown in Fig. 11. The 30° propatagium model is superior to all others, with a peak L:D value of 5.3. At low angles of attack, the basic wing model performs extremely poorly in comparison. Irregularities can be seen for the 10° and 20° model in Fig. 11 and at these angles of attack, the camber of the leading edge of the propatagium is raised above the frontal face of the wing spar. As a result, more of the air flow is in contact with the spar and the flow velocity is reduced. This effect is also seen for the basic model where the air is incident on the spar first, increasing pressure and reducing air velocity before it is in contact with the wing.

The increase in lift allowed by the inclusion of the pteroid bone is due to the increase in camber of the wing profile. At higher angles of attack, the entry angle of the airflow was reduced when compared to the angle of the propatagium. The propatagium also provides a larger wing area which increases lift, but also increases drag. The propatagium model was a clear improvement on the on the basic model, allowing it to operate better at higher angles of attack. This however came at the expense of flight efficiency as L:D ratios were reduced. The 30° model performed excellently due to the compromise between an increased camber and slim profile. The larger wing area afforded by the inclusion of the pteroid reduced the loading on the wing, therefore lowering the wing loading increases the lift produced at any give speed. This can be quantified using Gray's (1968) relation for calculating stall speed for animal locomotion given by:

$$V = \sqrt{\frac{2W}{C_L S \rho}} \tag{6}$$

Where W = weight (kg) and V = stall speed (m/s).

This data can help solve the problem of pterosaur take off dynamics. With the inclusion of the propatagium, the wing beat cycle of once per second would be sufficient (Stein 1976). Therefore the pterosaur would be able to alter the direction of the pteroid by flexing the pteroid muscle to suit the air velocity, without having to constantly flap its wings.

During flight, the propatagium allowed significant reductions in power requirements at low angles of attack. At angles above 10°, the increase in drag experienced by the wing due to the increased camber (see Fig. 5) suggests that no power reductions are available. According to Gray (1968), the power required by the pterosaur at a flying speed of Re 1.2 x 10^6 is given by;

$$Power = \frac{C_D}{C_L} \times Weight \times Velocity \tag{7}$$

The results show that the propatagium shared many similarities with the slats found on the leading edge of modern fixed wing aircraft which help to postpone stall and improve performance during manoeuvres. One of the key benefits of the pteroid bone was the improvement offered to flight control. Unlike a bird, the pterosaur did not have tail feathers to initiate turns and their limited flapping ability further restricted control over flight (Bramwell 1974) The majority of control therefore fell to the propatagium. During flight, extending the left pteroid bone whilst flexing the right would have increased the drag on the right wing initiating a roll, an operation not possible without the pteroid. Flexing both pteroids simultaneously would have sharply decreased the pterosaur's velocity so that it could quickly decrease its altitude. This ability, coupled with the increased bone rigidity in the sternum, the pterosaur was ideally suited for rapid descent and moderately heavy landing, with the propatagium decreasing stall speed and the fused bone structure absorbing impact.

Without a propatagium, the angle of attack required for landing would have increased the likelihood of stall and the speed required for landing would be increased (Fig. 14). With a propatagium, the significantly lower stall speed would suggest the pterosaur only had to face a moderate head wind, unfurl its propatagium and take off. The pterosaur wing can be likened to that of low loaded Rogallo wing gliders (McMasters 1976); with a low wing loading, their flight could have been very slow, requiring very few wing beats to stay airborne. Also, with the low power requirements shown in Fig. 15, the pterosaur could stay airborne almost indefinitely (Stein 1975) if required.

As mentioned in the results, the drag coefficient values are very poor when compared to Wilkinson's study. This can be attributed to flow separation occurring at the sharp edges of the wing. The abrupt redirection of flow leads to an increase in the turbulent kinetic energy thus precipitating an increase in turbulent eddies and vortices. The increase of pressure close to the boundary layer leads to an adverse pressure gradient forming at the wing particularly for the high θ_{pd} models. This is most evident in Fig. 16 where flow separation occurs above the wing spar. At lower angles of attack, flow separation occurs at the peak of the cheiropatagium.

The drag experienced by the wing is dependent on viscous forces whereas lift is a product of pressure forces. Fluent is able to model the lift experienced by the wing very well since the effects of the boundary layer have little effect on the pressure changes experienced by the wing. However, the program does have difficulty in predicting the position of the transition layer for irregular shapes and as such there is a major shortfall in the turbulent solver. This problem is exacerbated by the sharp edges of the wing profile since the solver assumes that the transitional layer is fixed to the wing profile. To reduce these effects, the solver could be run at much lower Reynold's numbers making the flow laminar but this would drastically change the lift results compared to those obtained in previous studies.

The solutions obtained using the k-ε solver were by far the most suitable (see appendix (d)). Utilising the inviscid solver caused the solution to diverge drastically, failing to provide a result even when reducing under-relaxation factors for pressure. The results presented by the k-ω model did not show any benefits in this situation, since its primary differences are the

incorporation of compressibility effects and low Reynold's number effects, which were not required in this investigation (Wilcox 1998).

By utilising periodic boundary conditions the airflow does not account for ground effects. Therefore the analysis carried out would only be suitable for flight high above the ground, away from the boundary layer effects caused by the.

Fig. 18 and 19 show how the wing spar affects the wing aerodynamics. Without a propatagium, the effective front face of the wing is the spar diameter. Therefore at the incidence of the flow with the spar, the pressure is greater due to the increased area of contact. This would increase the danger of stall occurring as the flow becomes reversed at the stagnation point. At very low flight speeds the pterosaur would not be able to sustain flight at low angles of attack. In order to stay airborne the pterosaur would require more wing beats thus requiring more energy.

Whilst on the ground the pteroid bone was flexed so that it was positioned towards the body. This allowed the pterosaur to fold its propatagium flush against the body and reduce the likelihood of the pteroid being damaged while walking. Fig. 20 shows the articulation of the pteroid in the forwards position and the range of movement it can undergo.
During flight the pressure on the propatagium would have stopped the pteroid from being orientated medially. The highest pressure is exerted at the pteroid joint in between the wing spar and the beginning of the propatagium (Fig. 13). Therefore it is the pteroid joint that absorbs most of the force exerted by flight (Wilkinson 2005).

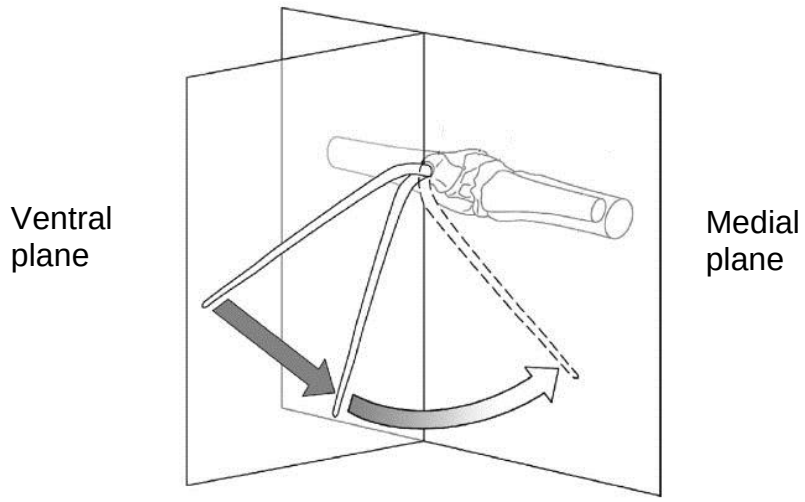

Fig. 20 – Orientation of pteroid adapted from Wilkinson (2005) showing the pteroid in flight position and folded postition

The findings of this study support those of Wilkinson (2005) in a number of key areas but there are some notable differences.
This study assumed an infinite length wing when being modelled thus negating the effects of induced drag. Since there is no wing tip no air flow can escape laterally away from the wing. In reality this would create a trailing vortex as the air escapes. Similarly, Wilkinson (2005) conducted his experiment in an enclosed test section thus negating induced drag also.

Modelling the wing profile using computational fluid dynamics (CFD) significantly reduced the number of factors affecting the airflow in comparison. Wilkinson (2005) required aluminium support structures to prop up the wing, which would have affected the airflow coming in contact with the wing. Also, by enclosing the section, the boundary layer of the tunnel walls would have affected the wing profile, but were not factored into his investigation. Since periodic boundary conditions were implemented in this study, boundary layer effects from the test section are negated.

Data for the wing profile was originally sourced from Unwin (1996) and scaled down for Wilkinson's (2005) investigation. However it is unlikely that the wing spar would scale up to the same extent as the wings (Bramwell & Whitfield 1974) meaning that it is probable that the wing spar is too large in this investigation. This is an important discrepancy when looking at the basic model because the effect of the wing spar is far greater without a propatagium (Fig. 18 and 19). Finally the extension and sail billow of the membrane in Wilkinson's (2005) study alters with each angle of attack. Whilst this would provide a more realistic simulation of a sail, there is no fossil evidence to suggest the actual mechanical properties of the wing, such as its rigidity. Therefore the behaviour of the pterosaur wing at full billow is completely unknown.

The results obtained from the 2D models have provided interesting results into flight mechanics of the pterosaurs. Further investigation of current fossil specimens is required to ultimately discover the correct anatomical arrangements of the wing structure. However, we may never determine the true dimensions of the wing membrane since the membrane has not been preserved in any of the fossilised specimens found because it is soft tissue, not bone.

Until these are found, there will be elements of speculation in all aerodynamic investigations. For this reason the use of 3D modelling may further compound errors, much like Soemmerring's (1817) incorrect wing leg attachment model. However combining data found in this investigation with Stein's (1975) findings would require 3D modelling and as such is the next stage in determining precisely how the pteroid bone would influence flight manoeuvres. The use of CFD in this investigation has many advantages over wind tunnel experiments. The majority of problems experienced by Wilkinson (2005), such as model instabilities, are negated with CFD and greater control over field variables is afforded thus improving experimental results. Fluent's main flaw is its limited drag prediction capability. Current data concerning wing properties is simply not available and as such basic assumptions concerning the wing must be made which may give rise to discrepancies in the reported drag values.

Conclusion

In conclusion, the use of an antero-ventral pteroid bone would have offered numerous flight advantages. The flight improvements shown were due to the increased camber of the wing allowing increased airflow at higher angles of attack The attachment of the propatagium to the pteroid afforded greater control over flight manoeuvres, delayed stall occurring and was necessary in allowing a stationary take off.

The increase in drag that was resultant of the pteroid would have limited the maximum flight speed of the pterosaur to approximately 15 m/s (Stein 1975). Looking at data for the minimum stall speed of the pterosaur (Fig. 14) suggests that the pterosaur would rarely fly so fast, since it was simply not necessary to maintain flight and would increase the power requirements. Controversy concerning the arrangement of the pteroid bone notwithstanding, it is clear from this study and previous works that the pteroid bone was an amazing appendage that radically changed pterosaur aerodynamics for the better.

Project plan

The project encompassed 15 weeks of work. The project plan can be seen in appendix (f). The expected time spent on each area of the study is shown in grey and the actual time spent is shown in blue. The earliest stages of the project, which included planning, theory and research presented more difficulties than expected due to the volume of data available. Whilst there was considerable data concerning pterosaurs in general, there were very few papers dealing with the pteroid bone in sufficient detail. The increased time spent on research postponed the practical work by almost two weeks. However progress with the modelling software was good, facilitating an easy transition from experimental results to investigation write up.

References

Barth, T. J., Jespersen, D
The design and application of upwind schemes on unstructured meshes. Technical Report AIAA-89-0366, AIAA 27th Aerospace Sciences Meeting, Reno, Nevada, 1989.

Bramwell, C. D., Whitfield, G. R.
Biomechanics of *Pteranodon*
Phil. Trans. R. Soc. B 1974, 267, 503-581

Frey, E., Reiss, J.
A new reconstruction of the pterosaur wing
N. Jb. Geol. Palaon. Abh. 1981, 161, 1-27

Gray, J.
Animal locomotion 1968
Weidenfield and Nicolson, London. P. 479

Greenhalgh, S., Curtis, H. C., Smith, B.
Aerodynamic properties of a two-dimensional inextensible flexible airfoil. 1984 AIAA J. 22, 865–870.
Wilkinson, M., Unwin, D. M., Ellington, C. P.
High lift function of the pteroid bone and forewing of pterosaurs

Proc. R. Soc. B 2005

Greenwalt, C. H.
Smithson. Misc. Collect. 1962, No. 2, 144

Hankin, E. A., Watson, D. M. S.
On the flight of Pterodactyls
Aeronautical Jour. Oct. 1914, 335

Hazelhurst, G. A., Rayner, J. M. V.
Flight characteristics of Triassic and Jurassic pterosauria: An appraisal based on wing shape
Paleobiology, Vol. 18, No. 4 (Autumn, 1992), 447-463

Padian, K., 1983
A functional analysis of flying and walking in pterosaurs
Paleobiology, Vol. 9, No. 3 (Summer, 1983), 218-239

Robbins, N.
Correspondence
Nature 2005, Vol. 425, p. 950

Rogers, G. F. C., Mayhew, Y. R.
Thermodynamic and transport properties of fluid
fifth edition 2003, Blackwell Publishing, p.16

Soemmerring, S. T. von.
A new reconstruction of *Ornithocephalus brevirostris of Vorwelt*
Denkschr. Kgl. Bayer. Akad. Wiss., 1817 p 89 - 104

Stein, R. S.
Dynamic analysis of *Pteranodon Ingens:* a reptilian adaptation to flight
*Journal of Paleontology*m, Vol. 49, No. 3 (May, 1975), 534-548

Stein, R. S., McMasters, J. H.,
Letters
Science, New series, Vol. 191, 1976 No. 4230 898-899

Unwin, D. M., Frey, E., Martill, D. M., Clarke, J. B., Riess, J.
Proceedings: Biological Sciences, Vol. 263, No. 1366 (Jan. 22, 1996), 45-52

Wellnhoffer, P.
The illustrated encyclopaedia of pterosaurs 1991a
pp. 50 – 56, London Salamander Books Ltd.

Wellnhofer, P.
Weitere Pterosaurierfunde Santana-Formation (Apt) der Chapada do Brasilien. Palaeontographica 1991b, A 215, 43–101.

D. C. Wilcox.
Turbulence Modeling for CFD.
DCW Industries, Inc., La Canada, California, 1998.

Williston, S. W.
The skull and hind extremity of *Pteranodon*
Amer. Naturalist. Vol. 25 1891, 25:1124

Appendix

(a)

Species	Mass (kg)	Wingspan (m)
Eudimorphodon ranzii	0.015	0.412
Dorygnathus banthensis	0.232	0.920
Campylognathoides zitteli	0.498	1.614
Scaphognathus crassirostris	0.043	0.480
Rhamphorhynchus longicaudus	0.013	0.404
R. muensteri	0.186	1.048
R. intermedius	0.025	0.456
R. gemmingi	0.24	1.052
Pterodactylus antiquus	0.096	0.595
P. micronyx	0.027	0.408
P. elegans	0.008	0.224
P. kochi	0.053	0.440
Pteranodon sp.	16.6	6.95

Table 6 – pterosaur weights and wingspans (Hazelhurst and Rayner, 1992)

(b)

Table 7 – Velocity components

Angle of attack (deg)	x vel. (m/s)	y vel (m/s)
0	19.93	0
2	19.92	0.70
4	19.88	1.39
6	19.82	2.08
8	19.74	2.77
10	19.63	3.46
12	19.49	4.14
14	19.34	4.82
16	19.16	5.49
18	18.95	6.16
20	18.73	6.82

(c)

Table 8 – Resultant force components

Angle of attack (deg)	Drag vector		Lift vector	
	x	y	x	y
0	1	0	0.000000	1
2	1	0.034921	-0.034921	1
4	1	0.069927	-0.069927	1
6	1	0.105104	-0.105104	1
8	1	0.140541	-0.140541	1
10	1	0.176327	-0.176327	1
12	1	0.212557	-0.212557	1
14	1	0.249328	-0.249328	1
16	1	0.286745	-0.286745	1
18	1	0.324920	-0.324920	1
20	1	0.363970	-0.363970	1

Table 8 – Resultant force components

(d) K-ε transport equations.

For k; (turbulent kinetic energy)

$$\frac{\partial}{\partial t}(\rho k) + \frac{\partial}{\partial x_i}(\rho k u_i) = \frac{\partial}{\partial x_j}\left[\left(\mu + \frac{\mu_t}{\sigma_k}\right)\frac{\partial k}{\partial x_j}\right] + P_k + P_b - \rho\epsilon - Y_M + S_k$$

For epsilon; (dissipation rate)

$$\frac{\partial}{\partial t}(\rho\epsilon) + \frac{\partial}{\partial x_i}(\rho\epsilon u_i) = \frac{\partial}{\partial x_j}\left[\left(\mu + \frac{\mu_t}{\sigma_\epsilon}\right)\frac{\partial \epsilon}{\partial x_j}\right] + C_{1\epsilon}\frac{\epsilon}{k}\left(P_k + C_{3\epsilon}P_b\right) - C_{2\epsilon}\rho\frac{\epsilon^2}{k} + S_\epsilon$$

Constants

$$C_{1\epsilon} = 1.44, \quad C_{2\epsilon} = 1.92, \quad C_\mu = 0.09, \quad \sigma_k = 1.0, \quad \sigma_\epsilon = 1.3$$

(e)

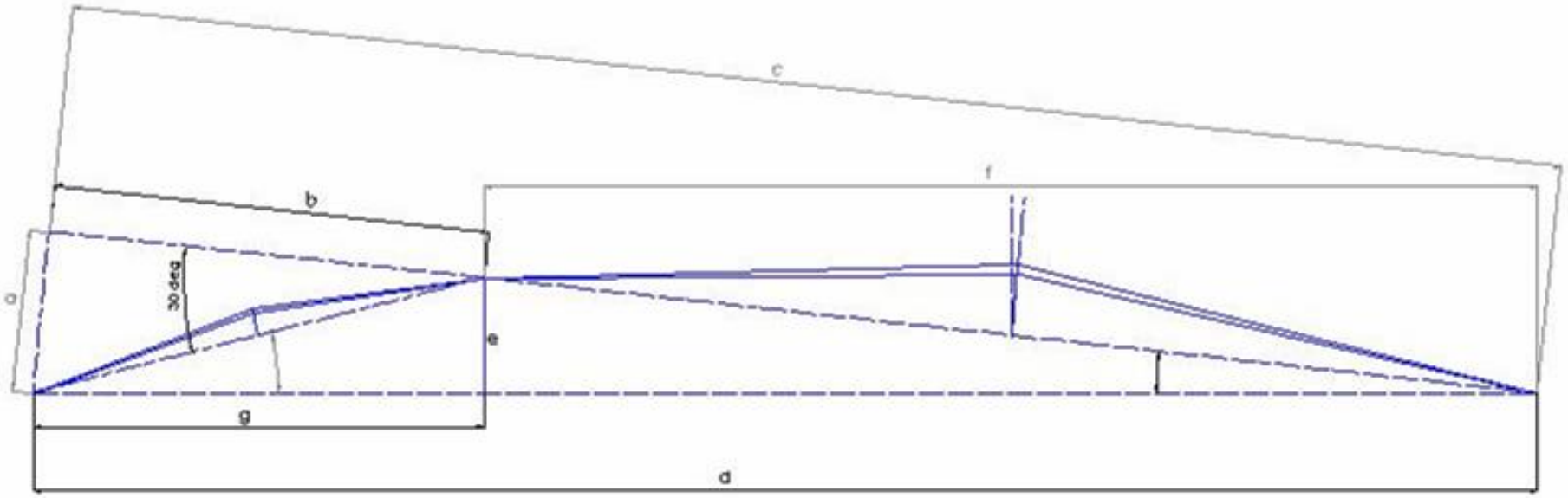

Fig. 21 – Dimensioned schematic of 30° propatagium model. a – g is the order in which each dimension was determined

(f)

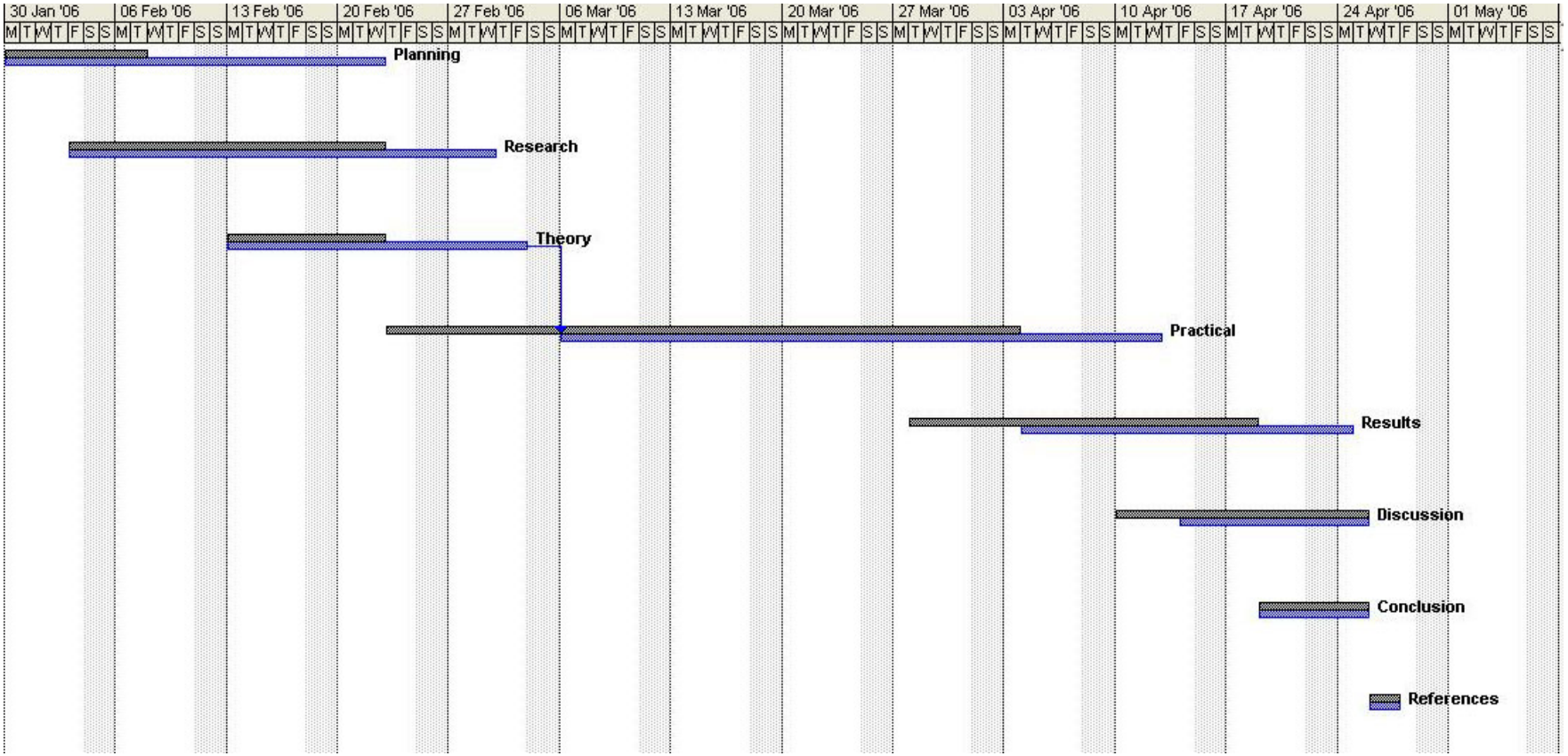

Fig 22 – Project plan. Projected plan is shown in grey with actual timings shown in blue